A new measurement of J/ψ suppression in Pb-Pb collisions at 158 GeV per nucleon

The NA50 Collaboration

B. Alessandro[10], C. Alexa[3], R. Arnaldi[10], M. Atayan[12], S. Beolè[10], V. Boldea[3], P. Bordalo[6,a], G. Borges[6], C. Castanier[2], J. Castor[2], B. Chaurand[9], B. Cheynis[11], E. Chiavassa[10], C. Cicalò[4], M.P. Comets[8], S. Constantinescu[3], P. Cortese[1], A. De Falco[4], N. De Marco[10], G. Dellacasa[1], A. Devaux[2], S. Dita[3], O. Drapier[9], J. Fargeix[2], P. Force[2], M. Gallio[10], C. Gerschel[8], P. Giubellino[10], M.B. Golubeva[7], M. Gonin[9], A. Grigoryan[12], S. Grigoryan[12], F.F. Guber[7], A. Guichard[11], H. Gulkanyan[12], M. Idzik[10,b], D. Jouan[8], T.L. Karavicheva[7], L. Kluberg[9], A.B. Kurepin[7], Y. Le Bornec[8], C. Lourenço[5], M. Mac Cormick[8], P. Macciotta[4], A. Marzari-Chiesa[10], M. Masera[10], A. Masoni[4], M. Monteno[10], A. Musso[10], P. Petiau[9], A. Piccotti[10], J.R. Pizzi[11], F. Prino[10], G. Puddu[4], C. Quintans[6], L. Ramello[1], S. Ramos[6,a], L. Riccati[10], A. Romana[9], H. Santos[6], P. Saturnini[2], E. Scomparin[10], S. Serci[4], R. Shahoyan[6,c], F. Sigaudo[10], M. Sitta[1], P. Sonderegger[5,a], X. Tarrago[8], N.S. Topilskaya[7], G.L. Usai[4], E. Vercellin[10], L. Villatte[8], N. Willis[8], T. Wu[8]

1 Università del Piemonte Orientale, Alessandria and INFN-Torino, Italy
2 LPC, Univ. Blaise Pascal and CNRS-IN2P3, Aubière, France
3 IFA, Bucharest, Romania
4 Università di Cagliari/INFN, Cagliari, Italy
5 CERN, Geneva, Switzerland
6 LIP, Lisbon, Portugal
7 INR, Moscow, Russia
8 IPN, Univ. de Paris-Sud and CNRS-IN2P3, Orsay, France
9 LLR, Ecole Polytechnique and CNRS-IN2P3, Palaiseau, France
10 Università di Torino/INFN, Torino, Italy
11 IPN, Univ. Claude Bernard Lyon-I and CNRS-IN2P3, Villeurbanne, France
12 YerPhI, Yerevan, Armenia

Abstract. We present a new measurement of J/ψ production in Pb-Pb collisions at 158 GeV/nucleon, from the data sample collected in year 2000 by the NA50 Collaboration, under improved experimental conditions with respect to previous years. With the target system placed in vacuum, the setup was better adapted to study, in particular, the most peripheral nuclear collisions with unprecedented accuracy. The analysis of this data sample shows that the (J/ψ) / Drell-Yan cross-sections ratio measured in the most peripheral Pb-Pb interactions is in good agreement with the nuclear absorption pattern extrapolated from the studies of proton-nucleus collisions. Furthermore, this new measurement confirms our previous observation that the (J/ψ) / Drell-Yan cross-sections ratio departs from the normal nuclear absorption pattern for semi-central Pb-Pb collisions and that this ratio persistently decreases up to the most central collisions.

1 Introduction

The suppression of the J/ψ yield in heavy ion collisions, predicted by Matsui and Satz [1], is commonly considered as one of the most interesting signals of the formation of a deconfined state of quarks and gluons in high-energy

heavy-ion collisions. The detection of J/ψ and ψ' mesons through their leptonic decay to a pair of muons is particularly interesting since muons are not affected by the strong interactions at play in the later stages of the collision evolution, when the light hadrons are formed.

The NA50 experiment is a high luminosity fixed target experiment at CERN, essentially dedicated to the study of dimuon production in Pb-Pb collisions at 158 GeV per nucleon. The analysis of the Pb-Pb data collected by NA50 in year 1995 showed [2,3] that the J/ψ production yield, with respect to the production of Drell-Yan dimuons, is ("anomalously") suppressed with respect to the "normal
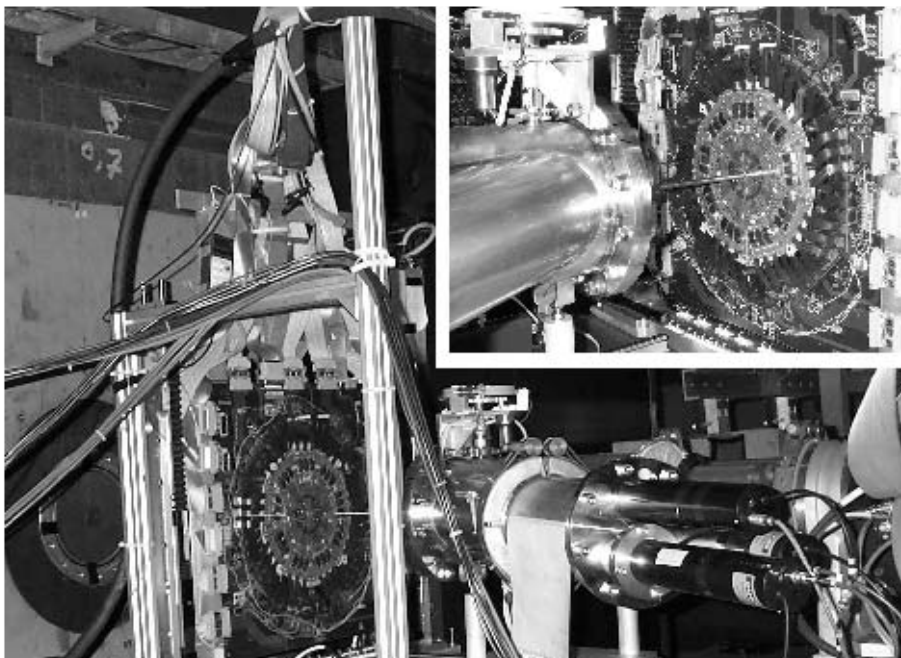

Fig. 1. The NA50 target region (beam entering from bottom right), including the target vacuum tank, the Multiplicity Detector and the upstream face of the carbon absorber; the Electromagnetic Calorimeter (not shown) with the BeO preabsorber in its center is inserted between the MD and the carbon absorber during data taking. The inset shows part of the target vacuum tank and the upstream face of the Multiplicity Detector's first plane (beam entering from left). During data taking conditions the target system is moved down-stream, almost touching the MD

nuclear absorption" pattern derived from measurements done in interactions induced by protons or light nuclei [4–6]. This "integrated" result was complemented by detailed studies of the J/ψ suppression pattern as a function of the centrality of the collision [7–9], with data collected in the years 1996 and 1998, which indicated that the extra suppression sets in for semi-central collisions and suggested that the departure from the normal absorption curve was setting in over a narrow range of centrality values.

A more detailed analysis of the Pb-Pb data revealed that peripheral interactions could be contaminated by Pb-air interactions, especially in the multi-target configuration used in the data taking period of 1996. We devoted the year 2000 data taking period to investigate further whether Pb-Pb peripheral collisions were really compatible with the results obtained from lighter collision systems, and to collect more statistics on several p-A systems, in order to establish a more precise normal absorption curve. It was also realized that, although the pattern describing their dependence as a function of the centrality of the collision remains essentially unaffected, the numerical values of the ratio of cross-sections $B_{\mu\mu}\sigma(J/\psi)/\sigma(DY)$ are somewhat sensitive to the specific parametrization used for the Parton Distribution Functions (PDFs). This happens because different PDFs give slightly different shapes for the Drell-Yan dimuon mass distribution and, therefore, as a result of the constraint imposed by the data in the high mass region, lead to a different Drell-Yan yield in the region $2.9 < M < 4.5$ GeV/c^2. Since the GRV 92 LO [10] PDFs were used for the analyses of the S-U data and of the 1995 Pb-Pb data, while the MRS A (Low Q^2) [11] PDFs (which take into account the isospin asymmetry in the quark sea, $\bar{u} \neq \bar{d}$, as determined by the NA51 experiment [12]) were taken for later data analyses, there is a systematic discrepancy between the corresponding results. To overcome this small inconsistency, all the data referred to in this paper,

both the Pb-Pb event samples and the lighter interacting systems used as reference, have been analyzed with a single set of PDFs. We have chosen the GRV 94 LO [13] PDFs, to take into account the quark sea asymmetry and to be consistent with the fact that the Monte Carlo event generators that we use are based on leading order calculations. Finally, we also report results normalized to the Drell-Yan yield in the muon pair mass range $4.2 < M < 7.0$ GeV/c^2, which have the advantage of being essentially insensitive to the PDFs chosen for the analysis.

In summary, this paper presents the measurement of the (J/ψ) / Drell-Yan cross-sections ratio, as a function of collision centrality, from data collected in year 2000, using our most recent data selection and analysis procedures. Preliminary results of this analysis have been previously presented in [14].

2 Experimental setup, event reconstruction and data selection

The experimental setup used by NA50 in the year 2000 included important improvements with respect to the one used in the previous Pb-Pb data taking periods of 1995, 1996 and 1998. The main change was the introduction of a new target system under vacuum [15] (see Fig. 1), which allowed a better rejection of out-of-target interactions and, in particular, of Pb-air interactions. For data selection, a new target identification algorithm was used, based on the silicon Multiplicity Detector [16] instead of the previous one, based on a system of quartz blades [17]. Furthermore, in order to identify almost simultaneous multiple interactions, a new method was developed based on the shape analysis of the signals of the Electromagnetic Calorimeter. Except for the new target system, the setup is described in detail in [2, 18]. Its main features are recalled hereafter.

The NA50 apparatus consists essentially of a set of beam and anti-halo counters, three centrality detectors, and a muon spectrometer. The intensity of the incoming ion beam is counted by a Beam Hodoscope (BH) made of 16 quartz slabs. Interactions occurring upstream of the target are vetoed by dedicated scintillator counters. Interactions in the target can be tagged by two quartz counters or by the two planes of silicon micro-strips of the Multiplicity Detector (MD), depicted in Fig. 1, which also count the charged particles produced in the angular range $1.9 < \eta < 4.2$. The other two centrality detectors are the Electromagnetic Calorimeter (EMC), which integrates the flux of neutral transverse energy E_T in the angular domain $1.1 < \eta < 2.3$, and the Zero-Degree Calorimeter (ZDC), which measures E_{ZDC}, the forward energy carried by the beam spectator nucleons ($\eta > 6.3$). The muon spectrometer starts with a hadron absorber, made of beryllium oxide, carbon and iron, followed by two sets of multi-wire proportional chambers, located upstream and downstream of an air-core toroidal magnet. The dimuon trigger is provided by 4 scintillator hodoscopes. A minimum bias (MB) trigger is defined by a minimal energy deposited in the ZDC and a "beam" trigger is provided by the BH, leading to a sample of events only constrained by the detection of an identified incident Pb ion. Data in year 2000 were taken with the 158 GeV/nucleon beam at 1–$1.4 \cdot 10^7$ ions/s, over 5 s bursts, and with a 4.0 mm thick Pb target, corresponding to 10 % of an interaction length (interaction probability: 9.6 %). In 35 days, we collected 135 million dimuon triggers on tape (plus additional triggers without target or at lower beam intensities) which led to 64 million reconstructed dimuons, of which 720 000 opposite-sign pairs in the J/ψ mass region (2.9–3.3 GeV/c^2). After data selection and background subtraction (see below) the number of useful dimuons in the J/ψ mass region was between 100 000 and 130 000 (depending on the particular definition of selection cuts).

The events were processed offline through a technically improved version of the software, featuring a higher track reconstruction efficiency [19,20] with respect to the version used for data taking periods before year 2000. The data selection proceeded as follows. First of all, parasitic interactions of the incident Pb ion in the BH were rejected using auxiliary scintillator counters. Then, multiple interactions were rejected by a temporal analysis of the signal in the EMC, allowing us to retain events where either one or two incident ions were detected in the BH, within a given time window, but only one ion interacted in the target. Some residual interaction pile-up events were further rejected by a diagonal band cut on the E_T–E_{ZDC} correlation, using the method described in [21] (Fig. 2).

The location of the primary interaction is determined by requiring the appropriate correlation between hits on the first and second planes of the MD. This method works for $E_T > 3$ GeV, and reaches full efficiency at $E_T \simeq 15$ GeV (see also [16]). It retains for further analysis significantly more peripheral events than the traditional target identification algorithm, based on quartz Cherenkov counters surrounding the target.

Muons originating downstream from the target (e.g. due to collisions in the BeO preabsorber or in the ZDC) are
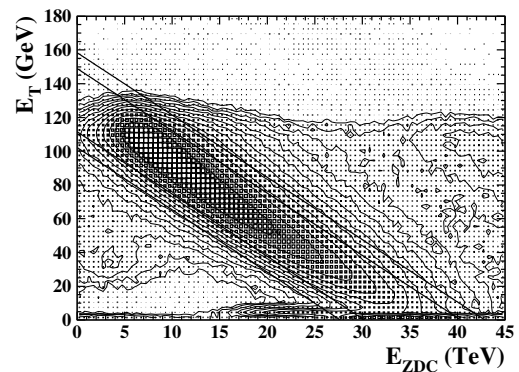

Fig. 2. Correlation between transverse and forward energy, showing $\pm 2\sigma$ and $\pm 3\sigma$ diagonal bands. Contours connect pixels of equal event density, ranging from 20 (external one) to 5024 (closest to the highest density), scaled with a constant factor

rejected by a cut on $p \cdot D_{Targ}$, where p is the momentum and D_{Targ} is the transverse distance between the extrapolated muon track at the target position and the beam axis. For the analysis of this paper, which is focused on high mass dimuons, the level of this "muon target cut" was set at 2 % of χ^2 probability for each muon (see [22] for details). We have verified that our results are stable when we increase the level of the cut up to 10 %, while of course the number of accepted dimuons is consequently reduced. The rather low level of the cut with respect to previous data taking periods is allowed by the improved experimental conditions in the year 2000 run, in particular the vacuum pipe extending inside the BeO preabsorber. We reach a quite effective rejection of the out-of-target events, which are especially numerous in the most peripheral centrality bin at masses around 2.5 GeV/c^2 (see also [14]).

Once the event selection is done, we can proceed with the definition of centrality classes. For this purpose we have used our three centrality detectors, with the corresponding variables: neutral transverse energy E_T, forward energy E_{ZDC} and charged particle multiplicity per unit of pseudo-rapidity at mid-rapidity, $(dN_{ch}/d\eta)|_{max}$, noted as N_{ch} in the following for simplicity of notation [23]. While E_T and N_{ch} are more directly correlated with the energy density of the collision, E_{ZDC} is a good estimator of the number of participant nucleons [9]. The centrality classes used in this paper are listed in Tables 1, 2 and 3. The bins are equidistant in the measured centrality estimator being used, except for the first (or first three in the case of N_{ch}) and last bin. These tables include the corresponding average and rms values of the number of participant nucleons, N_{part}, of the impact parameter, b, and of the average length of nuclear matter traversed by the (pre-resonant) charmonium state, L, all of them evaluated through a detailed Glauber calculation (see [24] for the Glauber formalism and [25] for an example of such an evaluation). For the Pb nuclear density we have used a 2-parameter Fermi distribution with a half-density radius of 6.624 fm and a diffuseness parameter of 0.549 fm (see [26] and reference Ja73 therein). The parameters quoted above only describe the proton distribution inside the Pb nucleus, and it is well known that neutrons are distributed differently. Since our reference,

Table 1. Centrality classes based on the transverse energy measurement. For each class we list the E_T range and average, together with the average and rms values of N_{part}, b and L

Class	E_T (GeV)		N_{part}		b (fm)		L (fm)	
	range	average	average	rms	average	rms	average	rms
1_T	3–15	10.6	34	13	11.8	0.7	4.44	0.72
2_T	15–25	20.4	70	13	10.3	0.5	5.94	0.42
3_T	25–35	30.3	104	14	9.2	0.4	6.84	0.33
4_T	35–45	40.2	138	16	8.2	0.4	7.51	0.27
5_T	45–55	50.2	172	17	7.3	0.4	8.02	0.23
6_T	55–65	60.1	206	18	6.5	0.4	8.43	0.20
7_T	65–75	70.1	240	19	5.6	0.5	8.76	0.17
8_T	75–85	80.1	274	20	4.8	0.5	9.02	0.15
9_T	85–95	90.1	308	21	3.9	0.6	9.22	0.12
10_T	95–105	100.0	341	20	2.8	0.7	9.38	0.11
11_T	105–150	111.5	367	15	1.7	0.7	9.48	0.06

Table 2. Centrality classes based on the forward energy measurement

Class	E_{ZDC} (TeV)		N_{part}		b (fm)		L (fm)	
	range	average	average	rms	average	rms	average	rms
1_F	31–36	33.0	44	27	11.6	1.4	4.70	1.27
2_F	27–31	28.9	76	35	10.3	1.3	5.89	1.18
3_F	23–27	25.0	119	39	8.8	1.2	7.04	0.88
4_F	19–23	21.0	170	39	7.4	1.0	7.92	0.59
5_F	15–19	17.0	223	38	6.1	0.9	8.56	0.39
6_F	11–15	13.0	276	35	4.7	0.9	9.01	0.26
7_F	7–11	9.1	330	31	3.2	1.0	9.32	0.16
8_F	0–7	5.7	365	19	1.8	0.9	9.47	0.09

Table 3. Centrality classes based on the measurement of the charged particle multiplicity

Class	$dN_{ch}/d\eta$		N_{part}		b (fm)		L (fm)	
	range	average	average	rms	average	rms	average	rms
1_N	1–41	22.4	39	21	11.7	1.0	4.58	0.97
2_N	41–81	62.0	70	25	10.4	0.9	5.83	0.78
3_N	81–120	101.2	101	29	9.3	0.9	6.70	0.66
4_N	120–173	147.2	138	34	8.3	0.9	7.44	0.57
5_N	173–226	200.0	179	38	7.2	1.0	8.06	0.48
6_N	226–279	253.0	220	41	6.2	1.0	8.53	0.40
7_N	279–332	305.7	260	43	5.1	1.1	8.88	0.32
8_N	332–385	358.1	297	41	4.1	1.2	9.13	0.25
9_N	385–438	410.1	327	36	3.2	1.2	9.30	0.18
10_N	438–835	487.9	352	27	2.3	1.1	9.42	0.13

the Drell-Yan process, is isospin-dependent, we have used a recent experimental measurement [27] of the "neutron halo" in heavy nuclei to define a 2-parameter Fermi distribution for neutrons, with the same half-density radius as for protons and a diffuseness parameter of 0.667 fm (for more details see [28]). The same model was adopted for the U nucleus with a half-density radius of 6.8054 fm and diffuseness parameters of 0.605 fm for protons and 0.786 fm for neutrons. The deformation of the U nucleus, which

interacts with random spatial orientation, was not taken into account.

3 Analysis method

Particle yields have been extracted by fitting the dimuon mass spectrum, for each centrality bin. First, a fit is performed to the $\mu^+\mu^+$ and $\mu^-\mu^-$ mass spectra, to deter-
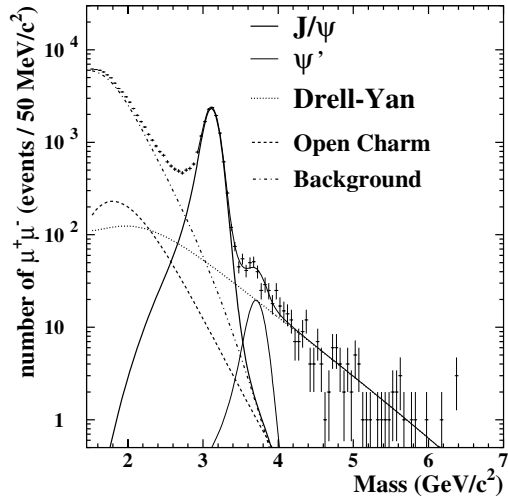
Fig. 3. Opposite-sign dimuon invariant mass spectrum for the centrality class $35 < E_T < 45$ GeV. The results from the fit are also shown

mine the combinatorial background, mostly due to π and K decays. The background in the opposite-sign dimuon sample is then parameterized according to the relation $N_{BG} = 2 \cdot R \cdot \sqrt{N^{++} \cdot N^{--}}$, where R can be taken as unity due to the absence of significant charge correlations in Pb-Pb collisions. The validity of this relation is granted by a fiducial cut which rejects muon pairs where any of the muons would not have been accepted if it had the opposite charge.

A multi-step fit to the $\mu^+\mu^-$ mass spectra (Fig. 3 shows an example) is then performed to extract the four signal contributions which are relevant for masses above 2.5 GeV/c^2, namely J/ψ, ψ', Drell-Yan and open charm. Finally, the acceptance corrections are applied, thus obtaining the cross-sections ratio $B_{\mu\mu}\sigma(J/\psi)/\sigma(DY)$. This ratio of two dimuon processes has the advantage of being insensitive to absolute normalizations (integrated luminosity) and to most of the experimental efficiencies, allowing us to directly compare these values to the normal nuclear absorption pattern derived from lighter collision systems. Furthermore, the Drell-Yan process is known (see e.g. Fig. 1 in [3] and Fig. 3 in [29]) to scale linearly with the product $A \times B$ of the projectile and target mass numbers, and therefore linearly with the number of binary nucleon-nucleon collisions.

The analysis is performed in the dimuon kinematical domain $0 < y_{cms} < 1$ and $-0.5 < \cos(\theta_{CS}) < 0.5$, where y_{cms} is the c.m.s. rapidity and θ_{CS} is the polar decay angle of the muons in the Collins-Soper reference frame [30].

For each of the four signal sources, muon pairs are generated and propagated through the NA50 detector using the NA38/NA50 Monte Carlo simulation package which implements the multiple scattering and energy loss processes of muons as done in GEANT 3.21 (see e.g. [31]). These events are then reconstructed using the standard NA50 reconstruction code in order to obtain the functional forms of each signal, needed for the fits to the measured invariant mass distributions, and their acceptances, needed for the calculation of the cross-sections ratio. For J/ψ and ψ' gener-

ation, we use a gaussian rapidity distribution with an r.m.s. value $\sigma = 0.6$ units [31] and a uniform $\cos(\theta_{CS})$ distribution. The transverse momentum is generated according to $K_1(M_T/T)$, where K_1 is the modified Bessel function and $T = 236$ MeV [31]. The Drell-Yan and open charm ($D\overline{D}$) contributions are calculated with PYTHIA 6.124 [32] using the GRV 94 LO [13] set of PDFs, as provided by the PDFLIB package [33]. In order to reproduce the measured p_T distributions, the width of PYTHIA's gaussian primordial k_T distribution has been set to 0.8 GeV/c for Drell-Yan and 1.0 GeV/c for open charm [34].

The simulated and reconstructed dimuon mass distributions are parameterized by empirical functional forms. Such functions are illustrated in Fig. 3, after adjustment to the measured invariant mass spectrum. A first approximation of the J/ψ and ψ' functional forms is obtained through the Monte Carlo procedure outlined above, which is meant to describe the detector momentum resolution, and the multiple scattering and energy loss in the materials (target and muon filter) crossed by the muons. However, the very high statistical precision of our data is incompatible with the imperfections of this Monte Carlo description. The calculated line shape of the J/ψ must be slightly adjusted in order to closely reproduce the measured J/ψ peak [19,20].

The line shape of the measured J/ψ resonance has been recently studied in detail [20], resulting in the use of a functional form which significantly improves the fit of the dimuon mass distributions. The new description of the J/ψ shape leads to a decrease in the level of the (J/ψ) / Drell-Yan cross-sections ratio by about 6 % with respect to our preliminary results [14], while the pattern as a function of centrality remains unchanged (for further details, see [15] and [35]).

The fit to the invariant mass distributions is made, using the maximum likelihood method, through a multi-step procedure. First, the combinatorial background in the $\mu^+\mu^-$ sample is estimated through a fit to the like-sign invariant mass spectra; then a fit in the region $2.9 < M < 8.0$ GeV/c^2 is performed to obtain a first approximation of the J/ψ, ψ' and Drell-Yan contributions; then the open charm contribution is estimated by a fit in the mass region $1.7 < M < 2.6$ GeV/c^2. Finally, in order to minimize potential fit-induced distortions of the highly sensitive Drell-Yan and ψ' components of the mass spectrum, the last fit is performed again in the region $2.9 < M < 8.0$ GeV/c^2 (see Fig. 3) with five free parameters, which are the J/ψ, ψ' and Drell-Yan normalizations, the J/ψ mass M_ψ and the J/ψ experimental width parameter σ_ψ. The fitted values are in the range 97–100 MeV/c^2 for σ_ψ, and in the range 3.110–3.112 GeV/c^2 for M_ψ.

Table 4. Acceptances of the experimental setup used in year 2000, for J/ψ → $\mu^+\mu^-$ and Drell-Yan dimuons, in the phase space window analyzed in this study

Process	Acceptance (%)
J/ψ	12.5
Drell-Yan (2.9–4.5 GeV/c^2)	13.8
Drell-Yan (4.2–7.0 GeV/c^2)	17.8

The acceptances of the NA50 detector, as calculated by our Monte Carlo simulations and in the phase space window mentioned above, are given in Table 4, for J/ψ and Drell-Yan dimuons (for the two mass regions considered in the present analysis). The relative systematic error on the acceptances is estimated to be 2%, while the statistical error is negligible.

4 Results

4.1 Summary of p-A results

In order to accurately establish the normal nuclear absorption pattern, data were collected, with the NA50 apparatus, using the CERN SPS 400 or 450 GeV proton beam and several different nuclear targets. Results from the first two of our three data samples have been recently published [19,29]. A publication concerning the results from the third data sample, taken at 400 GeV beam energy, is presently under preparation (see [36] for preliminary results).

In a previous publication [29] we presented the analyses of several data sets for the (J/ψ) / Drell-Yan cross-sections ratio. That study merged measurements done with 450 GeV protons (pp and pd from NA51; first 450 GeV p-A data samples from NA50), in the phase space domain $-0.5 < \cos\theta_{CS} < 0.5$ and $-0.4 < y_{cms} < 0.6$, with S-U measurements done at 200 GeV/nucleon (from NA38), in the domain $-0.5 < \cos\theta_{CS} < 0.5$ and $0.0 < y_{cms} < 1.0$. For consistency reasons, we have revisited that study and updated its results, including now the three p-A data samples of NA50, to establish the normal nuclear absorption curve needed for the present work. Moreover, S-U results are not included anymore in this study. It is very interesting to check if the measured S-U (J/ψ) / Drell-Yan results will become significantly different from the expected behaviour deduced using exclusively p-A measurements (see next subsection). To bring the analysis of those p-A data sets (and also of the S-U data set) in tune with the procedures used in the present study of the Pb-Pb data, the J/ψ and ψ' resonances, in the fits of the mass spectra, were described with the new line shapes [19,20] and we consistently used the GRV 94 LO PDF sets in all calculations. Moreover, the Monte Carlo simulation of J/ψ production in p-A collisions has been upgraded in order to reproduce more accurately the measured p_T and y distributions and thus obtain more precise J/ψ acceptance values for each individual data sample (for more details, see [28]).

The cross-sections ratios (J/ψ) / Drell-Yan for p-A collisions (including pp and pd results from NA51) are then fitted to a Glauber description of the normal nuclear absorption. The Glauber calculation is performed with three free parameters: the two independent normalizations (accounting for the different energy and kinematical conditions) and a common value for the J/ψ absorption cross-section. The fit leads to $\sigma_{abs} = 4.18 \pm 0.35$ mb, a value very similar to our previous result, 4.4 ± 0.5 mb (see [29]). Energy, rapidity domain and isospin corrections are then applied to scale down the normalization of the absorption curve from a pp system at 450 GeV to a Pb-Pb system at

158 GeV. To perform this scaling, we first compare the J/ψ absolute p-A cross-sections measured by NA50 at 450 and 400 GeV with the J/ψ absolute p-A cross-sections measured by NA38 and NA3 [37] at 200 GeV, in the phase space domain $-0.5 < \cos(\theta_{CS}) < 0.5$ and $0.0 < y_{cms} < 1.0$. If these absolute cross-sections are fitted with a common σ_{abs}, we obtain a value of 4.11 ± 0.43 mb, in excellent agreement with the value of 4.18 ± 0.35 mb quoted above and measured using (J/ψ) / Drell-Yan ratios at 450 and 400 GeV[1]. The same fit leads to a factor of 0.319 ± 0.025 (0.348 ± 0.027) which allows to scale down the J/ψ absolute cross-section from the 450 (400) GeV kinematical domain to the 200 GeV kinematical domain. In addition, an energy correction factor of 0.737 ± 0.006 is used to scale down the J/ψ cross-section from 200 to 158 GeV. This correction was obtained using the parametrization $\sigma_\psi(\sqrt{s}) = \sigma_0(1 - M_\psi/\sqrt{s})^n$, with the value $n = 12.8 \pm 0.3$ derived from a fit to available measurements. Furthermore, the change induced by the different $\sqrt{s}$ on the x_F window (for a fixed y_{cms} window: $0.0 < y_{cms} < 1.0$) and on the x_F distribution (parametrized as in [38]) implies a very small correction: 1.020 ± 0.013. The corresponding scaling factors for the Drell-Yan cross-section are computed at leading order using the GRV 94 LO PDF sets. The simultaneous change in energy and kinematical domains from 450 (400) GeV to 200 GeV amounts to 0.504 ± 0.012 (0.544 ± 0.010), while the change in energy and x_F for the much smaller drop between 200 and 158 GeV gives 0.7085 and 1.091, respectively. Finally, a factor 0.969 is applied to the absorption curve corresponding to the isospin change from pp to Pb-Pb.

The statistical uncertainty on the absorption curve as measured at the higher energies is $\pm 1\%$ at low centrality reaching $\pm 4\%$ at high centrality. Adding in quadrature the errors on the rescaling factors we obtain at 158 GeV an uncertainty of $\pm 8.3\%$ at low centrality reaching $\pm 9.0\%$ at high centrality. This normal nuclear absorption curve is reported in the following figures along with the Pb-Pb (J/ψ) / Drell-Yan data points.

4.2 Pb-Pb results

We now present the J/ψ suppression pattern for Pb-Pb interactions, as obtained from the data collected in year 2000. As in the past, we consider the cross-sections ratio (J/ψ) / Drell-Yan, where the Drell-Yan differential cross-section is integrated in the mass domain 2.9–4.5 GeV/c^2. The results from three independent analyses, using the centrality variables E_T, E_{ZDC} and N_{ch}, are shown in Figs. 4, 5 and 6, which also include the normal nuclear absorption curve, obtained as explained above. The corresponding numerical values are reported in Table 5. The results referred to the high mass Drell-Yan domain (4.2–7.0 GeV/c^2), which are less sensitive to the specific PDF sets used in the analysis, can be obtained by scaling up those reported in Table 5

---

[1] In the following, we adopt the value 4.18 ± 0.35 mb which is insensitive to most of the systematic uncertainties and, therefore, can be considered as our best estimate of σ_{abs}.

Table 5. Cross-sections ratio (J/ψ) / Drell-Yan, referred to the 2.9–4.5 GeV/c^2 Drell-Yan mass domain, for the Pb-Pb 2000 data, with three independent centrality estimators. Values for the Drell-Yan mass domain 4.2–7.0 GeV/c^2 may be obtained as explained in the text. Classes are defined in Tables 1, 2 and 3. Only statistical errors are given; systematic errors are negligible in comparison to statistical ones, as explained in the discussion session

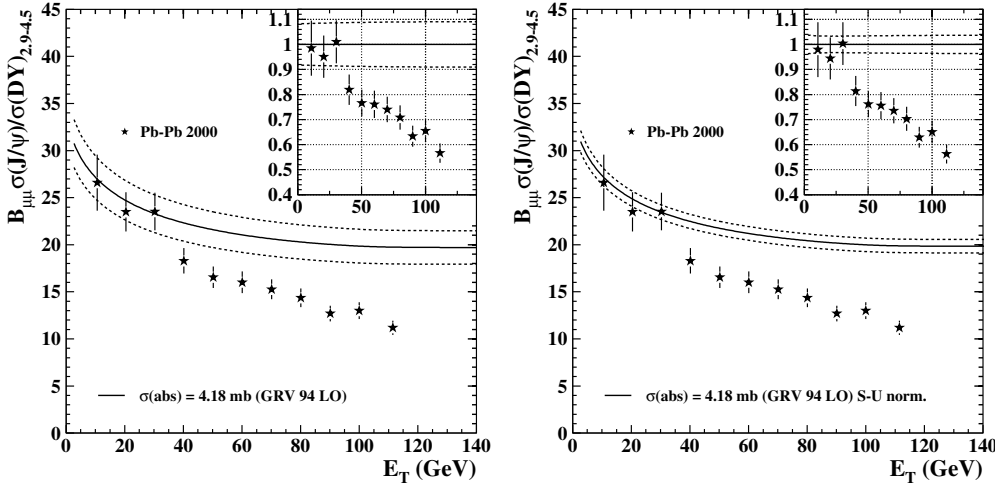| Class	$B_{\mu\mu}\sigma(J/\psi) / \sigma(DY)$	Class	$B_{\mu\mu}\sigma(J/\psi) / \sigma(DY)$	Class	$B_{\mu\mu}\sigma(J/\psi) / \sigma(DY)$
1_T	26.6 ± 3.0	1_F	26.3 ± 2.6	1_N	22.8 ± 2.6
2_T	23.5 ± 2.1	2_F	24.9 ± 2.1	2_N	25.8 ± 2.8
3_T	23.5 ± 2.0	3_F	20.3 ± 1.4	3_N	24.0 ± 2.4
4_T	18.3 ± 1.3	4_F	18.2 ± 1.2	4_N	18.2 ± 1.4
5_T	16.5 ± 1.1	5_F	16.2 ± 1.0	5_N	17.1 ± 1.2
6_T	16.0 ± 1.1	6_F	13.5 ± 0.7	6_N	15.7 ± 1.1
7_T	15.3 ± 1.0	7_F	13.6 ± 0.8	7_N	14.5 ± 1.0
8_T	14.4 ± 1.0	8_F	11.5 ± 1.0	8_N	15.5 ± 1.1
9_T	12.7 ± 0.8			9_N	14.8 ± 1.1
10_T	13.0 ± 0.9			10_N	12.5 ± 0.9
11_T	11.2 ± 0.8				

Fig. 4. The (J/ψ) / Drell-Yan cross-sections ratio as a function of transverse energy for the Pb-Pb 2000 data sample (left). The normal absorption curve is presented together with the combined error from the Glauber fit and the rescaling procedure (dashed curves). The inset shows the ratio Measured/Expected, i.e. data over normal nuclear absorption. The right panel presents the same data compared to the absorption curve computed using also S-U NA38 data for σ_{abs} determination and curve normalization

with the factor 7.96, the ratio between the Drell-Yan cross-sections integrated in the two mass domains.

Figure 4 (left) shows that the (J/ψ) / Drell-Yan ratio in peripheral Pb-Pb collisions is perfectly consistent with the pattern of normal nuclear absorption, as deduced from p-A collisions alone, with the appropriate normalization to 158 GeV/nucleon and to Pb-Pb isospin content. The departure from the normal absorption pattern at $E_T \sim$ 35 GeV and the non saturation at high E_T, already observed in previously published analyses, is also seen in this new sample of Pb-Pb collisions. The same observations can be made about the J/ψ absorption pattern as a function of the second centrality variable, E_{ZDC}, as shown in Fig. 5.

In Fig. 4 (right) we compare the Pb-Pb data to our previous determination of the absorption curve which made use of the NA38 S-U (J/ψ) / Drell-Yan ratios at 200 GeV together with the best estimates of the p-A data (either using J/ψ or (J/ψ) / Drell-Yan results) at higher energies [36]. This previous determination led to $\sigma_{abs} = 4.18 \pm 0.35$ mb. It is truly remarkable that this is exactly identical to the value presented above, and which was obtained through
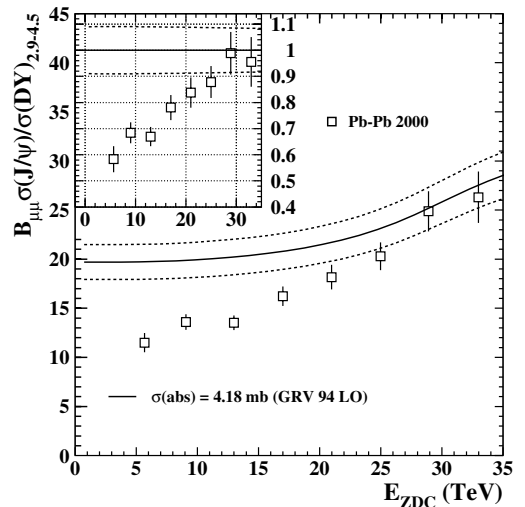

Fig. 5. The (J/ψ) / Drell-Yan cross-sections ratio as a function of forward energy for the Pb-Pb 2000 data sample. The inset shows the ratio Measured/Expected, i.e. data over normal nuclear absorption
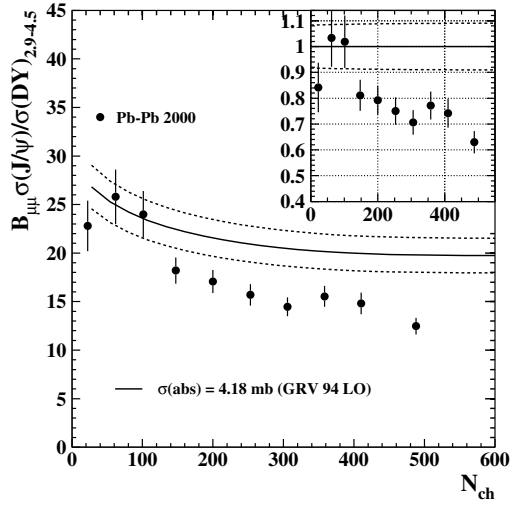
Fig. 6. The (J/ψ) / Drell-Yan cross-sections ratio as a function of charged multiplicity for the Pb-Pb 2000 data sample. The inset shows the ratio Measured/Expected, i.e. data over normal nuclear absorption

a rather different procedure, exclusively based on the 400 and 450 GeV proton-nucleus data. However, while the two determinations of σ_{abs} coincide, the new method leads to an absorption curve with a significantly larger error band (as seen in Fig. 4 left) originating from the uncertainty on the energy-rapidity rescaling factors, which are no longer constrained by the 200 GeV S-U results.

The analysis as a function of the third centrality variable, N_{ch}, has the unique feature that the charged particle multiplicity is evaluated in the rapidity window where the dimuons are measured by the muon spectrometer. From the (J/ψ) / Drell-Yan results displayed in Fig. 6 we observe that the suppression pattern is very similar to the one obtained with the E_T centrality variable. Note that the most peripheral data point corresponds to about half the statistics of the semi-central and central data points.

A comparison of the three independent analyses is presented in Fig. 7, using the average number of participant nucleons, N_{part}, as a common centrality variable. It is worth

recalling that E_T and the charged particle rapidity density at mid-rapidity are directly related to the energy density reached in the collision, through the Bjorken formula, while the forward energy measured in the ZDC is more strongly correlated to the geometry of the collision, being a simple and robust estimator of N_{part}. We have chosen N_{part} for the purpose of comparing our three independent analyses because it is well known that, at SPS energies, both E_T and N_{ch} are linearly proportional to N_{part}, as expected in the framework of the wounded nucleon model, up to the most central collisions (see, for instance, [24] and [25]).

The horizontal error bars in Fig. 7 represent the r.m.s. values of the N_{part} distribution in that bin, which depend on the experimental smearing, specific of each centrality variable. We see from this figure that the three (completely independent) centrality measurements give a very consistent picture. In particular, we do not see any evidence that the J/ψ suppression pattern looks different when looked as a function of variables related to particle production (E_T and N_{ch}) or as a function of simple geometry (E_{ZDC}).

In order to compare our Pb-Pb results with other (lighter) collision systems, we present in Fig. 8 (left) the (J/ψ) / Drell-Yan cross-sections ratio obtained in this analysis together with the results obtained in S-U (NA38) and p-A (NA50) interactions. The right panel of this figure shows the same data points after dividing by the function representing the normal nuclear absorption, using for the horizontal scale the average length L of nuclear matter traversed by the $c\bar{c}$ state. The length L has been evaluated as $\langle\rho(r)L\rangle/\rho_0$, where $\rho(r)$ is the nuclear density, normalized for each nucleus in order to give A nucleons upon integration, and ρ_0 is the average nuclear density, $0.17\,\mathrm{fm}^{-3}$. The figure shows how the J/ψ anomalous suppression clearly emerges from the reference line obtained exclusively from proton-nucleus data. We observe also that the S-U data points closely match the absorption curve determined from the p-A data, leaving very little room for anomalous absorption of the J/ψ in S-U collisions.

Finally, we present in Fig. 9 the (J/ψ) / Drell-Yan cross-sections ratio obtained in S-U (NA38) and Pb-Pb (NA50) interactions as a function of ϵ, the energy density averaged
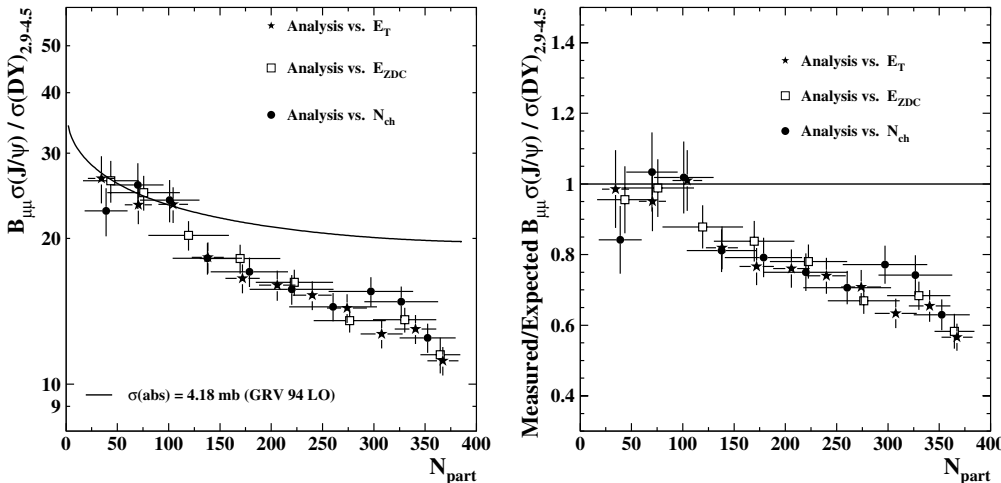

Fig. 7. The (J/ψ) / Drell-Yan cross-sections ratio as a function of N_{part} for three analyses of the Pb-Pb 2000 data sample, compared to (left) and divided by (right) the normal nuclear absorption pattern
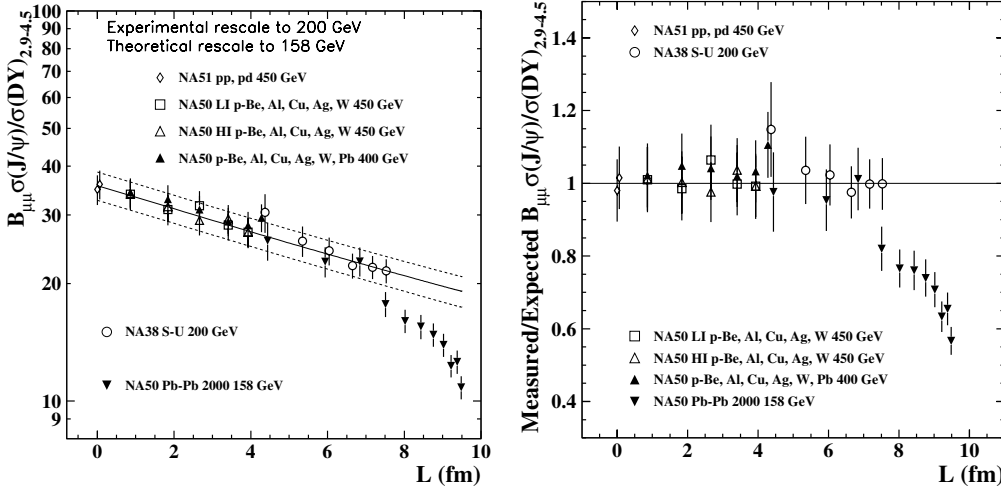
Fig. 8. The (J/ψ) / Drell-Yan cross-sections ratio vs. L, for several collision systems, compared to (left) and divided by (right) the normal nuclear absorption pattern. The measured data have been rescaled to 158 GeV/nucleon and for proton-proton isospin. The E_T data set was used for the Pb-Pb points
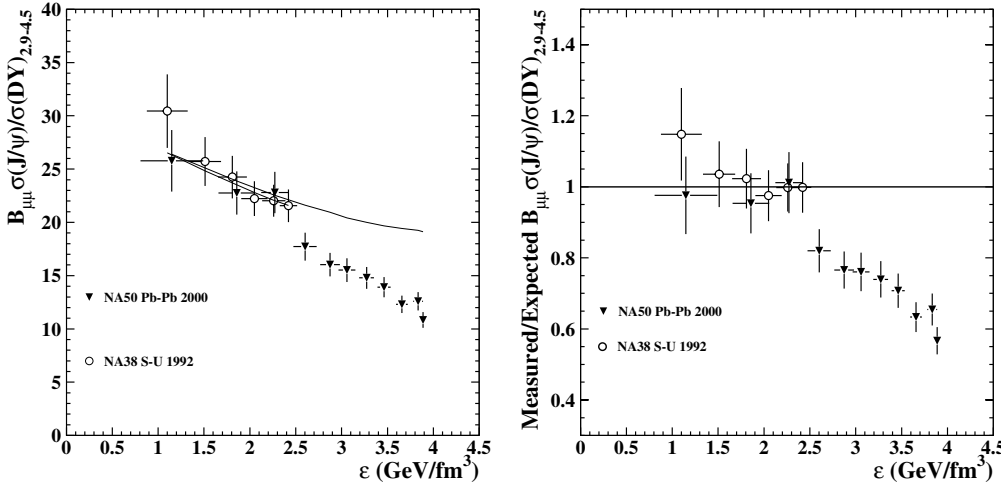

Fig. 9. The (J/ψ) / Drell-Yan cross-sections ratio as a function of the energy density, for the S-U and Pb-Pb collision systems, compared to (left) and divided by (right) the normal nuclear absorption pattern. The measured data have been rescaled to 158 GeV/nucleon and for proton-proton isospin. The E_T data set was used for the Pb-Pb points

over the whole transverse area of the collision, evaluated with the Bjorken formula:

$$\epsilon = \frac{\mathrm{d}E_T/\mathrm{d}\eta|_{\max}}{c\tau A_T} \quad ,$$

where A_T is the overlap area in the transverse plane and τ is the formation time, assumed to be 1 fm/c. We obtained the total transverse energy scaling up the measured (neutral) E_T by a factor 3. The different rapidity coverages of the NA38 and NA50 electromagnetic calorimeters have been taken into account, knowing that the $\mathrm{d}E_T/\mathrm{d}\eta$ distributions depend on the collision centrality.

This figure shows that the departure from the normal nuclear absorption curve sets in for energy densities around 2.5 GeV/fm^3, just above the values reached in the most central S-U collisions. The absorption curves for S-U and Pb-Pb in the left panel of Fig. 9 are slightly different because the relation between energy density and L (obtained from the Glauber calculation) depends on the colliding nuclei.

5 Discussion

We discuss first the statistical and systematical errors of the Pb-Pb 2000 results. Statistical errors in a given cen-

trality bin, coming from the fit to the mass spectrum, are in the range 5.5–8 %, and are, of course, dominated by the Drell-Yan statistics. We have evaluated the systematic errors coming from several sources (for details see [15,22,35]): (i) variation of the mass fit starting point, (ii) variation of the level of the muon target cut, (iii) variation of the E_T–E_{ZDC} correlation cut from $\pm 3\sigma$ to $\pm 2\sigma$, (iv) use of a counting technique using the number of signal events in the mass ranges 2.9–3.3 and 4.2–7.0 GeV/c^2, with subtraction of the number of Drell-Yan events in the first mass range. The point-to-point systematic error from the above sources was found to be negligible when compared to the statistical error.

Another systematic effect comes from the choice of PDFs for the Drell-Yan process (influencing both the mass fit and the acceptance calculation), which affects the overall normalization of our results while leaving unchanged the shape of the suppression pattern as a function of centrality. We have compared our standard choice of PDF (GRV 94 LO) with more recent PDFs computed at leading order, namely GRV 98 LO [39], MRST (central gluons) LO [40] and CTEQ 5L [41]. We have studied the effect of changing the Drell-Yan functional form while keeping the same normalization in the 4.2–7.0 GeV/c^2 mass region, as imposed by our data. The maximum change in the Pb-Pb
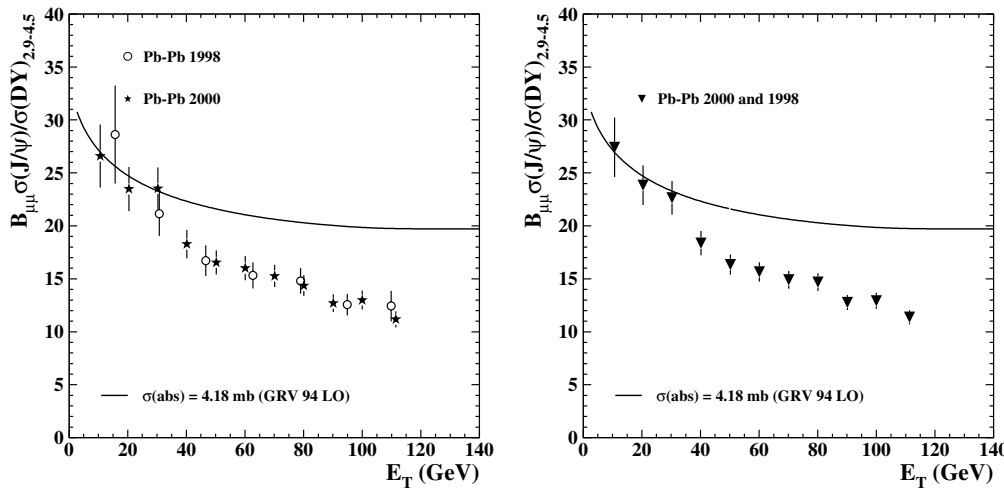
Fig. 10. Comparison between 1998 and 2000 results: separate (J/ψ) / Drell-Yan cross-sections ratios from 1998 and 2000 (left) and weighted average (right), as a function of transverse energy

(J/ψ) / Drell-Yan cross-sections ratio is 3.5 % (for comparison, using the sets GRV 92 LO and MRS A (Low Q^2) quoted in the introduction, we obtain a change of 0.8 % and 10 %, respectively).

We now discuss briefly how the Pb-Pb 2000 results on the (J/ψ) / Drell-Yan cross-sections ratio, presented above, compare with our results from previous Pb-Pb data taking periods.

We consider the 1998 data sample, collected with an experimental setup similar to the one used in year 2000 except for the vacuum around the target, and find excellent agreement, as shown in the left panel of Fig. 10, after repeating the analysis with our most recent procedures (see [22]). The introduction of the vacuum around the target region has brought a considerable increase in statistics of peripheral events. The weighted average of the two analyses (where data of year 1998 have been rebinned using the year 2000 centrality classes) is presented in the right panel of Fig. 10. The resulting suppression pattern suggests two different suppression regimes, one for peripheral and one for central reactions. The observed transition between these two regimes, including the smearing due to the resolution of the e.m. calorimeter which amounts here to 8%, extends over a range of about 15 GeV in $E_{\rm T}$.

6 Conclusion

We have analyzed the most recent NA50 Pb-Pb data sample, collected in year 2000 under improved experimental conditions, which allowed us to extend the analysis of the (J/ψ) / Drell-Yan cross sections ratio down to very peripheral interactions using only dimuon triggers. We have used three different centrality estimators, namely transverse energy, forward energy and charged particle multiplicity. Our analysis shows that peripheral Pb-Pb interactions, with impact parameter $b > 8.5$ fm, exhibit a J/ψ production yield in agreement with the normal nuclear absorption pattern, with $\sigma_{\rm abs} = 4.18$ mb, derived from an extensive study of p-A collisions. For smaller impact parameter values we observe a departure from the normal absorption curve,

followed by a persisting decrease up to the most central Pb-Pb collisions.

References

1. T. Matsui, H. Satz, Phys. Lett. B **178**, 416 (1986)
2. M.C. Abreu et al. (NA50 Collaboration), Phys. Lett. B **410**, 327 (1997)
3. M.C. Abreu et al. (NA50 Collaboration), Phys. Lett. B **410**, 337 (1997)
4. M.C. Abreu et al. (NA51 Collaboration), Phys. Lett. B **438**, 35 (1998)
5. M.C. Abreu et al. (NA38 Collaboration), Phys. Lett. B **449**, 128 (1999)
6. M.C. Abreu et al. (NA38 Collaboration), Phys. Lett. B **466**, 408 (1999)
7. M.C. Abreu et al. (NA50 Collaboration), Phys. Lett. B **450**, 456 (1999)
8. M.C. Abreu et al. (NA50 Collaboration), Phys. Lett. B **477**, 28 (2000)
9. M.C. Abreu et al. (NA50 Collaboration), Phys. Lett. B **521**, 195 (2001)
10. M. Glück et al., Z. Phys. C **53**, 127 (1992)
11. A. D. Martin et al., Phys. Rev. D **51**, 4756 (1995)
12. A. Baldit et al. (NA51 Collaboration), Phys. Lett. B **332**, 244 (1994)
13. M. Glück et al., Z. Phys. C **67**, 433 (1995)
14. L. Ramello et al. (NA50 Collaboration), Nucl. Phys. A **715**, 243 (2003)
15. C. Castanier, Ph.D. Thesis, Université Blaise Pascal, Aubière, France, 2003. Available at http://cern.ch/NA50/theses.html

16. B. Alessandro et al., Nucl. Instrum. Methods A **493**, 30 (2002)
17. F. Bellaiche et al., Nucl. Instrum. Methods A **398**, 180 (1997)
18. R. Arnaldi et al., Nucl. Instrum. Methods A **411**, 1 (1998)
19. B. Alessandro et al. (NA50 Collaboration), Eur. Phys. J. C **33**, 31 (2004)
20. R. Shahoyan, Ph.D. Thesis, Instituto Superior Técnico, Lisbon, Portugal, 2001; Available at http://cern.ch/NA50/theses.html
21. C. Quintans, Ph.D. Thesis, Instituto Superior Técnico, Lisbon, Portugal, 2002; Available at http://cern.ch/NA50/theses.html
22. H. Santos, Ph.D. Thesis, Instituto Superior Técnico, Lisbon, Portugal, 2004. Available at http://cern.ch/NA50/theses.html
23. M.C. Abreu et al. (NA50 Collaboration), Phys. Lett. B **530**, 33 (2002)
24. D. Kharzeev et al., Z. Phys. C **74**, 307 (1997)
25. M.C. Abreu et al. (NA50 Collaboration), Phys. Lett. B **530**, 43 (2002)
26. C.W. de Jager et al., Atomic Data and Nuclear Data Tables **14**, 479 (1974)
27. A. Trzcinska et al., Phys. Rev. Lett. **87**, 082501-1 (2001)
28. B. Alessandro et al. (NA50 Collaboration), Charmonium production and nuclear absorption in p-A interactions at 400 GeV, in preparation
29. M.C. Abreu et al. (NA50 Collaboration), Phys. Lett. B **553**, 167 (2003)
30. J.C. Collins, D.E. Soper, Phys. Rev. D **16**, 2219 (1977)
31. C. Lourenço, Ph.D. Thesis, Instituto Superior Técnico, Lisbon, Portugal, 1995; Available at http://cern.ch/NA38/na38thesis.html
32. T. Sjöstrand et al., Comput. Phys. Commun. **135**, 238 (2001)
33. H. Plothow-Besch, Int. J. Mod. Phys. A **10**, 2901 (1995)
34. L. Capelli, Ph.D. Thesis, Université Claude Bernard, Lyon, France, 2001; Available at http://cern.ch/NA50/theses.html
35. F. Sigaudo, Ph.D. Thesis, Università di Torino, Turin, Italy, 2003; Available at http://cern.ch/NA50/theses.html
36. G. Borges (for the NA50 Collaboration), J. Phys. G: Nucl. Part. Phys. 30 (2004) S1351
37. J. Badier et al. (NA3 Collaboration), Z. Phys. C **20**, 101 (1983)
38. G.A. Schuler, Habilitationschrift, Univ. Hamburg, Germany, 1994, CERN-TH-7170-94 (hep-ph/9403387)
39. M. Glück et al., Eur. Phys. J. C **5**, 461 (1998)
40. A.D. Martin et al., Eur. Phys. J. C **4**, 463 (1998)
41. H.L. Lai et al. (CTEQ Collaboration), Eur. Phys. J. C **12**, 375 (2000), hep-ph/9903282